Structural Engineering and Mechanics, Vol. 11, No. 4 (2001) 423-442 423
DOI: http://dx.doi.org/10.12989/sem.2001.11.4.423

Second-order analysis of planar steel frames considering the effect of spread of plasticity

Liang-Jenq Leu† and Ching-Huei Tsou‡

Department of Civil Engineering, National Taiwan University, Taipei, 10617 Taiwan, R.O.C.

Abstract. This paper presents a method of elastic-plastic analysis for planar steel frames that provides the accuracy of distributed plasticity methods with the computational efficiency that is greater than that of distributed plasticity methods but less than that of plastic-hinge based methods. This method accounts for the effect of spread of plasticity accurately without discretization through the cross-section of a beam-column element, which is achieved by the following procedures. First, nonlinear equations describing the relationships between generalized stresses and strains of the cross-section are derived analytically. Next, nonlinear force-deformation relationships for the beam-column element are obtained through lengthwise integration of the generalized strains. Elastic-plastic flexibility coefficients are then calculated by differentiating the above element force-deformation relationships. Finally, an elastic-plastic stiffness matrix is obtained by making use of the flexibility-stiffness transformation. Adding the conventional geometric stiffness matrix to the elastic-plastic stiffness matrix results in the tangent stiffness matrix, which can readily be used to evaluate the load carrying capacity of steel frames following standard nonlinear analysis procedures. The accuracy of the proposed method is verified by several examples that are sensitive to the effect of spread of plasticity.

Key words: second-order analysis; steel frames; spread of plasticity; flexibility matrix.

1. Introduction

With regard to the modeling of distributed plasticity or spread of plasticity in steel structures, plastic zone methods, often referred to as distributed plasticity or spread of plasticity methods, are the most accurate one but they are computation intensive. In contrast, the conventional plastic hinge method, often referred to as the lumped plasticity method, is computation efficient. However, it often overestimates the ultimate strength of structures (e.g. White *et al.* 1993), especially for structures whose members bend about the minor axis. The overestimation results from the fact that the effect of member plastification, being modeled using zero-length plastic-hinges located at the member ends, may not be accurately considered. To overcome the drawback, several modified plastic-hinge models have been proposed recently. These include the notional-load plastic-hinge (Liew *et al.* 1994), tangent-modulus plastic-hinge (White 1993), and refined plastic-hinge approaches (Liew *et al.* 1993a, b). A detailed discussion of the above three plastic-hinge based approaches was given by White *et al.* (1993). According to White *et al.*, the refined plastic-hinge method is the most accurate one. However, the above three approaches were all developed to evaluate the in-plane

† Associate Professor
‡ Formerly Graduate Student

strength of structures; three-dimensional behaviors such as flexural-torsional effects were not considered.

In plastic zone analyses (e.g. Clarke *et al*. 1992, Zhou and Chen 1994, Teh and Clarke 1999), members need to be discretized along their length and through their cross-section to model the gradual spreading of plastic zones. Discretization is often achieved using longitudinal fiber elements considering only the uniaxial stress-strain relationship. Hence, methods of this type are also referred to as fiber element methods. Although very accurate and applicable in analyzing spatial steel frames, spread-of-plasticity methods are more computation intensive than plastic-hinge based methods.

Recently, Attalla *et al*. (1994) and Attalla (1995) proposed another accurate inelastic analysis procedure, called the quasi-plastic-hinge approach. The computational efficiency of this approach is greater than that of distributed plasticity methods since discretization through the cross-section of a beam-column element is not required; however, the efficiency is still less than that of plastic-hinge based methods. Moreover, it can be applied to carry out inelastic analysis for both planar and spatial steel frames although only planar frames are discussed here. The reader is referred to Attalla (1995) regarding the application of this approach in spatial steel frames including how to model the effect of non-uniform torsional-flexural buckling.

The derivation of the quasi-plastic-hinge approach starts from the inelastic model that expresses the inelastic cross-sectional generalized strains, including curvature and centroidal axial strain, as functions of the generalized stresses, containing moment and axial force. The results obtained from plastic zone methods with respect to a W8×31 section are used to calibrate the inelastic model. The resulting curvature and axial strain equations are then integrated numerically along the members to obtain the member deformations, including end rotations and axial deformation, which in turn can be used to formulate first the elastic-plastic flexibility matrix and then the elastic-plastic stiffness matrix.

The quasi-plastic-hinge method is very promising in that it can account for the effect of spread of plasticity accurately for both planar and spatial steel frames and its computational effort is less than that required in plastic zone methods. However, it has two drawbacks. First, the inelastic model is calibrated using a W8×31 section; the accuracy is unclear when this model is applied in analyzing frames that are made of sections of other sizes. Second, the derived elastic-plastic flexibility matrix is unsymmetrical, which cannot be justified. This study aims at resolving the above two problems and only planar steel frames will be considered.

2. Generalized stress-strain relationships

Consider a simply supported beam-column subjected to a compressive axial force P and end moments M_1 and M_2 as shown in Fig. 1. If the curvature and the centroidal axial strain distributions along the length of the member are known, then by integrating the curvature distribution or equivalently by employing the conjugate beam theorem, the end rotations α_1 and α_2 can be obtained. Similarly, the axial shortening δ can be obtained by integrating the centroidal axial strain distribution. As will be explained later, the curvature and centroidal axial strain at any section of the member are explicit functions of the member forces P, M_1, and M_2. Hence, the member deformations δ, α_1, and α_2 are also functions of P, M_1, and M_2.

In this section, we discuss briefly how to derive the moment-curvature-axial force and centroidal axial strain-curvature-axial force relationships for I-shaped sections with the residual stress

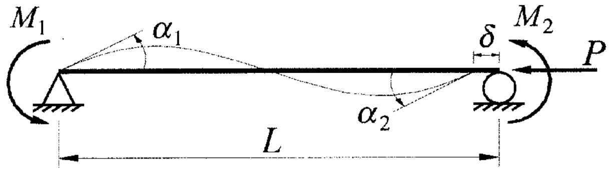

Fig. 1 Simply supported beam-column

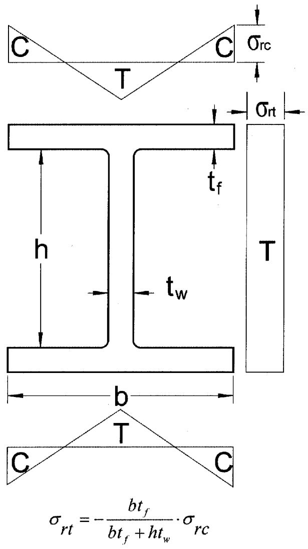

Fig. 2 Residual stress pattern

distribution being depicted in Fig. 2 (Galambos and Ketter 1959). Because the residual stress distribution is symmetric, the derived relationships are applicable for both positive and negative moments.

2.1 Normalized moment-curvature-axial force relationship

According to the extent of yielding, six and eight configurations of partially plastified sections can be distinguished for bending about the major and minor axes, respectively, as depicted in Figs. 3 and 4. Also, depending on the magnitude of axial forces, a cross-section under increasingly applied moment has the evolutionary paths as shown in Figs. 5 and 6, for the major- and minor-axis bending, respectively. Note that in Fig. 5, configuration IV-1 starts from $\bar{h}=h/2$ and $-h/2 \le \bar{g} \le h/2$; configuration IV-2 $\bar{g}=-h/2$ and $-h/2 \le \bar{h} \le h/2$. Also in Fig. 6, configuration IV-1 starts from $\bar{h}=t_w/2$ and $-b/2 \le \bar{g} \le t_w/2$; configuration IV-2 $\bar{g}=-b/2$ and $-b/2 \le \bar{h} \le t_w/2$; configuration VIII-1 $\bar{h}=-t_w/2$ and $-b/2 \le \bar{g} \le -t_w/2$; and configuration VIII-2 $\bar{g}=-b/2$ and $-b/2 \le \bar{h} \le -t_w/2$.

For each of the above configurations, the normalized moment-curvature-axial force (m–ϕ–p) relationship, $m(\phi, p)$, has been derived and given explicitly in Tsou (1997). Note that $m=M/M_y$, where M=moment and M_y=yield moment; $\phi=\Phi/\Phi_y$, where Φ=curvature, $\Phi_y=M_y/EI$, E=Young's modulus, and I=second moment of inertia; $p=P/P_y$, where $P_y=A\sigma_y$, A=cross-sectional area, and σ_y= yield stress. The procedure for deriving the (m–ϕ–p) relationship is briefly stated as follows.

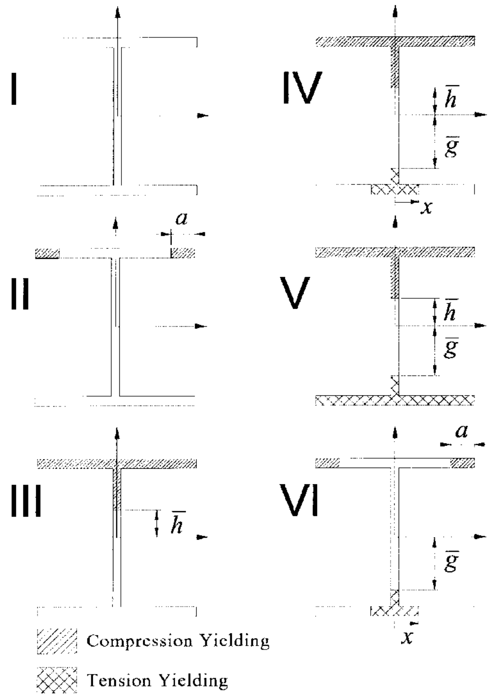

Fig. 3 Partially plastified sections due to major-axis bending

First, let

$$\varepsilon_{rc}=\sigma_{rc}/E \tag{1}$$

$$\varepsilon_{rt}=\sigma_{rt}/E \tag{2}$$

where σ_{rc} and σ_{rt} are the maximum magnitude of the compressive and tensile residual stresses as depicted in Fig. 2. Next, assume that

$$\sigma_{rc}=R_1\sigma_y \tag{3}$$

$$\sigma_{rt}=R_2\sigma_y \tag{4}$$

As the residual stresses are self-equilibrating, the following relation holds:

$$R_2=-\frac{bt_f}{bt_f+ht_w}R_1 \tag{5}$$

where b=width of the flange, t_f=thickness of the flange, h=depth of the web, and t_w=thickness of the web. In this study, R_1=0.3 is used; this value is quite typical for hot-rolled I-shaped sections according to Galambos and Ketter (1959). Note that compressive strains and stresses are assumed to be positive.

Consider, for example, configuration VIII of Fig. 4. The corresponding strain distribution over the cross-section is shown in Fig. 7(a). To facilitate the determination of the associated stress distribution, let's define the strain caused by the residual stresses as a "virtual strain" field, whose

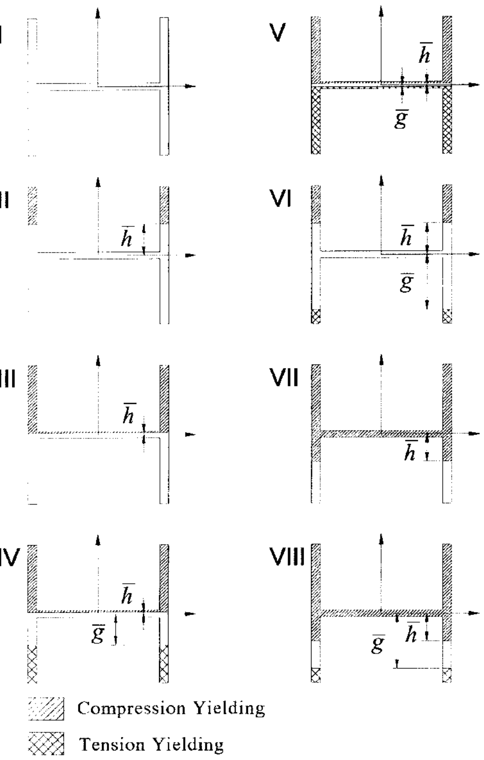

Fig. 4 Partially plastified sections due to minor-axis bending

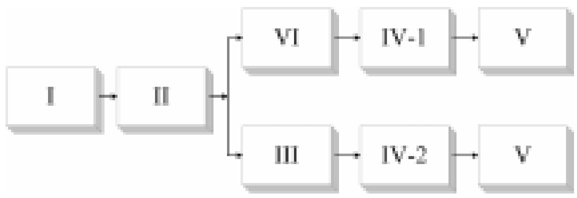

Fig. 5 Spread-of-plasticity paths for major-axis bending

distribution is depicted in Fig. 7(b). Adding together the actual strain and the virtual strain results in the total virtual strain shown in Fig. 7(c), from which the stress distribution of Fig. 7(d) can be easily obtained.

The virtual strain field shown in Fig. 7(b), denoted by $\varepsilon_v(y)$, can be written as

$$\varepsilon_v(y)=\varepsilon_{rt}+\frac{2(\varepsilon_{rc}-\varepsilon_{rt})}{b}y \quad \text{for} \quad y \geq 0 \tag{6a}$$

$$\varepsilon_v(y)=\varepsilon_{rt}+\frac{2(-\varepsilon_{rc}+\varepsilon_{rt})}{b}y \quad \text{for} \quad y \leq 0 \tag{6b}$$

Because $\bar{g}<0$ and $\bar{h}<0$ for configuration VIII of Fig. 4, the virtual strains at the interfaces between the elastic and plastic regions, defined in Fig. 7(b), can be expressed as

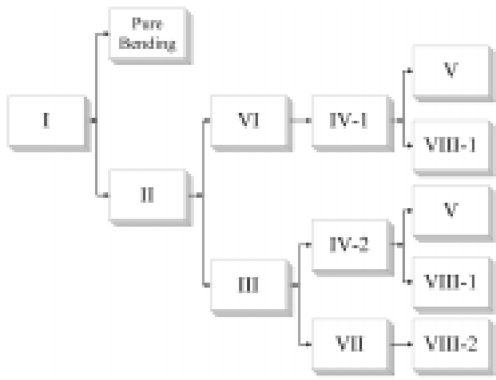

Fig. 6 Spread-of-plasticity paths for minor-axis bending

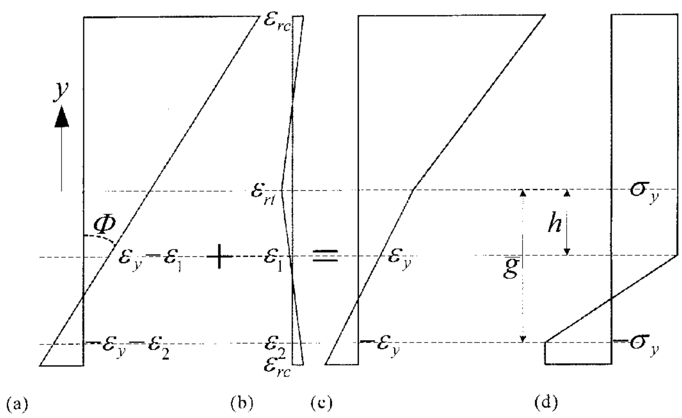

Fig. 7 (a) strain distribution, (b) "virtual strain distribution" due to residual stresses, (c) total virtual strain distribution, (d) stress distribution

$$\varepsilon_1=\varepsilon_v(\bar{h})=\varepsilon_{rt}+\frac{2(-\varepsilon_{rc}+\varepsilon_{rt})}{b}\bar{h} \tag{7}$$

$$\varepsilon_2=\varepsilon_v(\bar{g})=\varepsilon_{rt}+\frac{2(-\varepsilon_{rc}+\varepsilon_{rt})}{b}\bar{g} \tag{8}$$

Note that $\bar{g}$ and $\bar{h}$ are the y coordinates of the above interfaces as indicated in Fig. 4.

Based on the Bernoulli-Euler hypothesis that plane sections remain plane or according to Fig. 7(a), it can be derived that

$$\bar{g}=\bar{h}-\frac{2\varepsilon_y-\varepsilon_1+\varepsilon_2}{\Phi} \tag{9}$$

where $\varepsilon_y=\sigma_y/E$, the yield strain. By substituting Eqs. (7) and (8) into Eq. (9) and making use of the relations: $\varepsilon_{rc}=R_1\varepsilon_y$ and $\varepsilon_{rt}=R_2\varepsilon_y$, one obtains

$$\bar{g}=\frac{-b+\bar{h}(\phi-R_1+R_2)}{\phi-R_1+R_2} \tag{10}$$

From Fig. 7(a), the strain distribution due to sectional axial force and moment can be written as

$$\varepsilon(y)=\varepsilon_y-\varepsilon_1+(y-\bar{h})\Phi \tag{11}$$

With the use of Eqs. (6a, b) and (11), the stress distribution in the elastic core, which is the region from $\bar{g}$ to $\bar{h}$ of Fig. 7(d), can be evaluated by Hooke's law as follows:

$$\sigma(y)=E\varepsilon(y)+E\varepsilon_v(y) \tag{12}$$

Referring to Fig. 7(d), the normalized axial force and moment can be written, respectively, as

$$\begin{aligned} p=\frac{\int_A \sigma\, dA}{P_y}=&\left[\int_{-\frac{b}{2}}^{\bar{g}}(-\sigma_y)2t_f\,dy+\int_{\bar{g}}^{\bar{h}}(E\varepsilon+E\varepsilon_v)2t_f\,dy+\int_{\bar{h}}^{-\frac{t_w}{2}}(\sigma_y)2t_f\,dy\right.\\ &\left.+\int_{-\frac{t_w}{2}}^{\frac{t_w}{2}}\sigma_y(h+2t_f)dy+\int_{\frac{t_w}{2}}^{\frac{b}{2}}(\sigma_y)2t_f dy\right]\frac{1}{(ht_w+2bt_f)\sigma_y} \end{aligned} \tag{13}$$

$$\begin{aligned} m=\frac{\int_A \sigma y\, dA}{M_y}=&\left[\int_{-\frac{b}{2}}^{\bar{g}}(-\sigma_y)2t_f\,ydy+\int_{\bar{g}}^{\bar{h}}(E\varepsilon+E\varepsilon_v)2t_f\,y\,dy+\int_{\bar{h}}^{-\frac{t_w}{2}}(\sigma_y)2t_f\,ydy\right.\\ &\left.+\int_{-\frac{t_w}{2}}^{\frac{t_w}{2}}\sigma_y(h+2t_f)ydy+\int_{\frac{t_w}{2}}^{\frac{b}{2}}(\sigma_y)2t_f ydy\right]\frac{1}{\left(\frac{ht_w^3}{6b}+\frac{b^2t_f}{3}\right)\sigma_y} \end{aligned} \tag{14}$$

By making use of Eqs. (1)-(4), (6b)-(8), and (10)-(12), Eqs. (13) and (14) can be simplified as follows:

$$\begin{aligned} p&=p(\phi,\bar{h};R_1,R_2,h,t_w,b,t_f)\\ &=\frac{2t_fb+(t_wh-4t_f\bar{h})(\phi-R_1+R_2)}{(\phi-R_1+R_2)(2bt_f+ht_w)} \end{aligned} \tag{15}$$

$$\begin{aligned} m&=m(\phi,\bar{g},\bar{h};R_1,R_2,h,t_w,b,t_f)\\ &=\frac{3b^3-12b\bar{g}^2+(\phi-R_1+R_2)(-8\bar{g}^3+12\bar{g}^2\bar{h}-4\bar{h}^3)}{(2b^3t_f+ht_w^3)} \end{aligned} \tag{16}$$

In Eqs. (15) and (16), R_1,R_2,h,t_w,b, and t_f are considered as parameters.

Eq. (15) expresses p as a function of ϕ and $\bar{h}$; by rearranging the equation, $\bar{h}$ can be written as a function of ϕ and p as follows:

$$\begin{aligned} \bar{h}&=\bar{h}(\phi,\,p;R_1,\,R_2,\,h,\,t_w,\,b,\,t_f)\\ &=\frac{b}{2(\phi-R_1+R_2)}-\frac{bp}{2}+\frac{ht_w(1-p)}{4t_f} \end{aligned} \tag{17}$$

Finally, substituting $\bar{g}$ from Eqs. (10) into (16) and then using (17) yields the normalized moment-curvature-axial force relationship, $m(\phi, p)$.

In addition to $m(\phi, p)$, one also needs to know the starting ϕ and m for a give value of p when formulating the elastic-plastic flexibility matrix of a beam-column element, as will be seen later. Depending on the starting condition, configuration VIII of Fig. 4 can be further classified into two types; one, called VIII-1, begins with $\bar{h}=-t_w/2$ and $-b/2\le\bar{g}\le-t_w/2$, and the other, called VIII-2, starts from $\bar{g}=-b/2$ and $-b/2\le\bar{h}\le-t_w/2$. For configuration VIII-1, the starting ϕ, denoted by $\phi(p)_{0,VIII\text{-}1}$, can be obtained by solving Eq. (17) knowing that $\bar{h}=-t_w/2$; this results in

$$\phi(p)_{0,VIII\text{-}1}=\frac{(R_1-R_2)(2bpt_f+hpt_w-2t_f t_w)+2bt_f+R_2ht_w}{2pbt_f-(1-p)ht_w-2t_f t_w} \tag{18}$$

Similarly for configuration VIII-2, obtaining $\bar{h}$ first from Eq. (17) with $\bar{g}=-b/2$, and then solving for ϕ from Eq. (17) yields

$$\phi(p)_{0,VIII\text{-}2}=-R_1+R_2+\frac{-bt_f+bt_f(R_1-R_2)^2-(1+R_1-R_2)c}{(p-1)(2bt_f+ht_w)} \tag{19a}$$

where

$$c=\sqrt{bt_f[2bt_f(3-4p)(R_1-R_2)+bt_f(1+R_1^2+R_2^2)+4ht_w(R_1-R_2)(1-p)]} \tag{19b}$$

The starting normalized moment, denoted by $m(p)_0$, can be obtained simply by substituting the starting $\phi(p)_0$ into the $m(\phi, p)$ relationship.

In summary, for each configuration, one needs to derive the $m(\phi, p)$ relationship such as Eq. (16) (after substituting $\bar{g}$ from Eq. 10 and then $\bar{h}$ from Eq. 17). In addition, the starting normalized curvature for a given normalized axial force, $\phi(p)_0$, is also needed. Finally, the starting normalized moment is evaluated using $m(p)_0=m(\phi, p)|_{\phi=\phi(p)_0}$.

All the above derivations are carried out using MATHEMATICA (Wolfram 1991). The $m(\phi, p)$, $\phi(p)_0$, and $m(p)_0$ for other configurations of Figs. 3 and 4 can also be derived similarly. The resulting explicit (but lengthy) expressions are not given here for brevity; they are available in Tsou (1997).

2.2 Normalized centroidal axial strain- curvature-axial force relationship

A byproduct of the above normalized (m–ϕ–p) relationship, $m(\phi, p)$, is the normalized centroidal axial strain-curvature-axial force (ε_0–ϕ–p) relationship, $\bar{\varepsilon}_0(\phi, p)$, where the normalized centroidal axial strain is defined as

$$\bar{\varepsilon}_0=\varepsilon_0/\varepsilon_y \tag{20}$$

From Fig. 7(a), the centroidal axial strain can be expressed as

$$\varepsilon_0=\varepsilon_y-\varepsilon_1-\bar{h}\Phi \tag{21}$$

By substituting ε_0 from Eqs. (21) into (20) first, then making use of Eqs. (1)-(4) and (7), and noting that $\Phi=\phi\Phi_y$, where $\Phi_y=\varepsilon_y/(b/2)$ for the minor-axis bending, one obtains

$$\bar{\varepsilon}_0 = 1 - R_2 - \frac{2\bar{h}}{b}(\phi - R_1 + R_2) \tag{22}$$

Finally, substituting $\bar{h}$ from Eq. (17) into (22) yields $\bar{\varepsilon}_0(\phi, p)$.

2.3 Branching normalized axial loads

Depending on the magnitude of axial forces, a cross-section under increasingly applied moment has the evolutionary paths shown in Figs. 5 and 6, for the major- and minor-axis bending, respectively. How do we know, for a particular value of axial force, along which path the section will evolve? For example, a section with configuration II of Fig. 6 will enter into either configuration VI or III; which one is correct? This can be answered by comparing the starting normalized curvatures of these two configurations. Obviously, if $\phi(p)_{0,VI} < \phi(p)_{0,III}$, the section will enter into configuration VI and if $\phi(p)_{0,VI} > \phi(p)_{0,III}$, it will enter into configuration III.

Another way of determining the right configuration is by use of the branching normalized axial load which is defined as the normalized axial load at which the starting normalized curvatures of two branching configurations are the same. For example, solving for p from $\phi(p)_{0,VI} = \phi(p)_{0,III}$ yields the branching normalized axial load of configurations VI and III as follows:

$$p_{W,VI,III} = \frac{b(bt_f + ht_w) - t_w(bt_f + 2ht_w)(R_1 - R_2) - ht_w^2 - t_f t_w^2(1 + R_1 - R_2)}{(b + t_w)(2bt_f + ht_w)} \tag{23}$$

where the subscript w means minor-axis bending. If $p < p_{W,VI,III}$, the section will enter into configuration VI; otherwise, configuration III. Note that in Figs. 5 and 6, upper paths correspond to lower axial loads.

Similarly, we can determine the other two branching normalized axial loads associated with Fig. 6 as follows:

$$p_{W,IV-2,VII} = \frac{2b(bt_f + ht_w) + bt_f t_w(2 + R_1 - R_2) - t_f t_w^2(R_1 - R_2)}{2b(2bt_f + ht_w)} \tag{24}$$

$$p_{W,V,VIII-1} = \frac{ht_w}{2bt_f + ht_w} \tag{25}$$

For the paths shown in Fig. 5, which are associated with the major-axis bending, the only one branching normalized axial load can be determined in a similar manner; it is given by

$$p_{S,VI,III} = \frac{(2bh^2 t_f + h^3 t_w)(R_1 - 2R_2) + bht_f^2(3R_1 - 5R_2) - (bt_f^3 - h^2 t_f t_w)(1 - R_1 + R_2)}{2h(h + t_f)(2bt_f + ht_w)} \tag{26}$$

where the subscript s means major-axis bending.

3. Beam-column element

3.1 Member force-deformation relationships

Consider again the simply supported beam-column of Fig. 1, the normalized moment along its length can be written as

$$m(x)=-m_1+\frac{x}{L}(m_1+m_2) \tag{27}$$

where m_1 and m_2 are the normalized moments at the left and right ends, respectively. The conjugate beam theory is employed here to determine the end rotations α_1 and α_2 as functions of m_1, m_2, and p through the following steps.

1. Determine the evolutionary path by comparing p with the branching normalized axial loads.
2. Calculate the starting normalized moment, $m(p)_0$, and the starting normalized curvature, $\phi(p)_0$, for each configuration on the path determined using Step 1.
3. Determine to which configurations the end sections belong; this could be done easily by comparing m_1 and m_2 with the starting normalized moments calculated using Step 2.
4. Obtain the normalized end curvatures ϕ_1 and ϕ_2 by solving iteratively the $m(\phi, p)$ relationships corresponding to the end sections from the given m_1, m_2 and p.
5. Divide the normalized curvature distribution into $(2n+2)$ increments as shown in Fig. 8, where the part between $-\phi_e$ and ϕ_e is elastic; the value of n=10 is used in this study. Let the sampling normalized curvatures be represented by $\phi^{(k)}$ (k=1, 2n+3); notice that $\phi^{(1)}=\phi_1$, $\phi^{(n+1)}=-\phi_e$, $\phi^{(n+2)}=0$, $\phi^{(n+3)}=\phi_e$, and $\phi^{(2n+3)}=\phi_2$. For each $\phi^{(k)}$, the corresponding configuration can be determined by comparing its value with the starting normalized curvatures calculated using Step 2.
6. Calculate the normalized moment, $m^{(k)}$(k=1, 2n+3), associated with $\phi^{(k)}$(k=1, 2n+3) using the $m(\phi, p)$ relationship corresponding to the configuration determined at Step 5. Note that $m^{(1)}=-m_1$ and $m^{(2n+3)}=m_2$.
7. Determine the position, $x^{(k)}$(k=1, 2n+3), corresponding to $m^{(k)}$(k=1, 2n+3) using $x^{(k)}=L(m^{(k)}+m_1)/(m_1+m_2)$, which is obtained by rearranging Eq. (27).
8. Finally, α_1 and α_2 can be obtained by the conjugate beam theory assuming that the normalized curvature distribution is piecewise linear, constructed by connecting the sampling points of Step 5. Namely,

$$\alpha_1=-\frac{\Phi_y}{L}\sum_{k=1}^{2n+2} A^{(k)}L^{(k)} \tag{28}$$

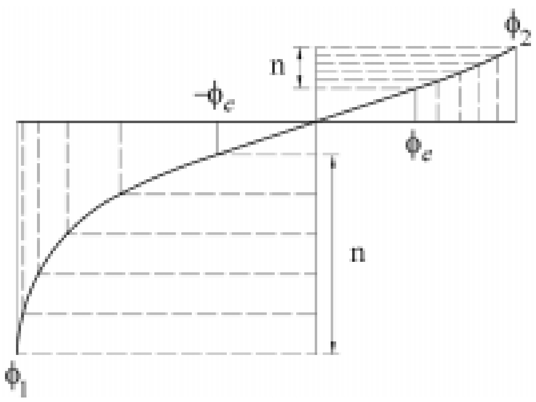

Fig. 8 Discretization of normalized curvature along the element length

$$\alpha_2 = \frac{\Phi_y}{L} \sum_{k=1}^{2n+2} A^{(k)} \left(L - L^{(k)} \right) \tag{29}$$

where $A^{(k)}$ is the area under the normalized curvature curve that is between $x^{(k)}$ and $x^{(k+1)}$, and $L^{(k)}$ is the horizontal distance between the centroid of $A^{(k)}$ and the right end ($x=L$); they are given, respectively, by

$$A^{(k)} = \frac{1}{2} \left[\phi^{(k)} + \phi^{(k+1)} \right] \left[x^{(k+1)} - x^{(k)} \right], \quad k=1, 2n+2 \tag{30}$$

$$L^{(k)} = L - x^{(k)} - \frac{\phi^{(k)} + 2\phi^{(k+1)}}{3(\phi^{(k)} + \phi^{(k+1)})} \left(x^{(k+1)} - x^{(k)} \right), \quad k=1, 2n+2 \tag{31}$$

Similarly, using the normalized centroidal axial strain-curvature-axial force relationship, $\bar{\varepsilon}_0(\phi, p)$, the normalized axial strain at $x^{(k)}$ (k=1, $2n$+3), $\bar{\varepsilon}_0{}^{(k)}$($k$=1, $2n$+3), can be determined. The axial shortening δ is then obtained by integrating ε_0 ($=\bar{\varepsilon}_0 \varepsilon_y$), which is assumed to be piecewise linear; namely

$$\delta = \frac{1}{2} \sum_{k=1}^{2n+2} \left[\bar{\varepsilon}_0{}^{(k)} + \bar{\varepsilon}_0{}^{(k+1)} \right] \left(x^{(k+1)} - x^{(k)} \right) \varepsilon_y \tag{32}$$

3.2 Elastic-plastic flexibility matrix and tangent stiffness matrix

The member deformations δ, α_1, and α_2 can be considered as functions of the member forces P, M_1, and M_2 as discussed in the above subsection. The incremental relationship between them can therefore be written as:

$$\begin{Bmatrix} \Delta\delta \\ \Delta\alpha_1 \\ \Delta\alpha_2 \end{Bmatrix} = \begin{bmatrix} \partial\delta/\partial P & \partial\delta/\partial M_1 & \partial\delta/\partial M_2 \\ \partial\alpha_1/\partial P & \partial\alpha_1/\partial M_1 & \partial\alpha_1/\partial M_2 \\ \partial\alpha_2/\partial P & \partial\alpha_2/\partial M_1 & \partial\alpha_2/\partial M_2 \end{bmatrix} \begin{Bmatrix} \Delta P \\ \Delta M_1 \\ \Delta M_2 \end{Bmatrix} \tag{33}$$

or expressed in matrix form as

$$\{\Delta u_n\} = [d]\{\Delta f_n\} \tag{34}$$

where $\{\Delta u_n\}$ and $\{\Delta f_n\}$ denote the increments of the member deformations and forces, respectively, and $[d]$ represents the elastic-plastic flexibility matrix. In this study, the coefficients of $[d]$ are calculated by the finite difference method assuming a 0.01 percent difference. For example,

$$d_{32} = \frac{\alpha_2(P, M_1 + \Delta M_1, M_2) - \alpha_2(P, M_1, M_2)}{\Delta M_1} \tag{35}$$

where $\Delta M_1 = 0.0001 M_1$ if $M_1 \neq 0$ and $\Delta M_1 = 0.0001 M_2$ when M_1=0.

The above elastic-plastic flexibility matrix for the supported beam-column of Fig. 1 can be used to derive the elastic-plastic stiffness matrix for the unsupported element of Fig. 9 having the degrees of freedom of $\{\Delta u\} = \{\Delta u_1, \Delta v_1, \Delta\theta_1, \Delta u_2, \Delta v_2, \Delta\theta_2\}^T$ as follows (McGuire *et al.* 2000):

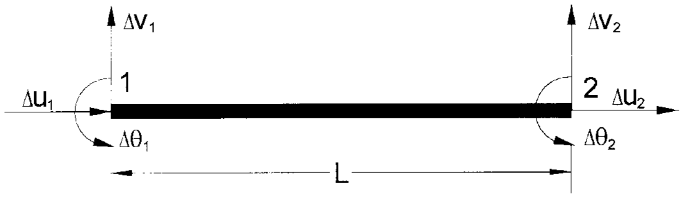

Fig. 9 unsupported beam-column element

$$[k_{ep}]=[T]^T[d]^{-1}[T] \tag{36}$$

where

$$[T]=\begin{bmatrix} 1 & 0 & 0 & -1 & 0 & 0 \\ 0 & 1/L & 1 & 0 & -1/L & 0 \\ 0 & 1/L & 0 & 0 & -1/L & 1 \end{bmatrix} \tag{37}$$

The second-order or geometric nonlinearity effect is incorporated into the analysis by use of the conventional geometric stiffness matrix $[k_g]$, available in Yang and Chiou (1987). Therefore, the tangent stiffness matrix takes the form:

$$[k_t]=[k_{ep}]+[k_g] \tag{38}$$

4. Nonlinear analysis procedure

Nonlinear analysis of structures is often carried out by an incremental-iterative procedure. The procedure consists of two major phases. The first one is to compute the increment of the displacement vector, which is often referred to as the predictor phase. The second one is referred to as the corrector phase; it is aimed at calculating the member end forces and at checking whether the equilibrium between the member end forces and the applied external loads is satisfied. If the equilibrium is not satisfied, iteration is started and continued until the magnitude of the unbalanced force vector is small. Otherwise, begin next loading step (increment) and the whole procedure is repeated. For a detailed discussion on the above aspects, the reader is referred to Yang and Kuo (1994).

The Newton-Raphson method in conjunction with the generalized displacement control technique proposed by Yang and Shieh (1990) are employed in the predictor phase since the technique can deal with nonlinear problems with limit points. In the corrector phase, the member end forces are updated according to the equation:

$$\{f_2\}=\{f_1\}+\{\Delta f\} \tag{39}$$

where $\{\Delta f\}$ are the increments of the member end forces that correspond to the degrees of freedom of Fig. 9. Also, $\{f_2\}$ and $\{f_1\}$ denote, respectively, the member end forces of the current and the last calculated configurations. The calculation of $\{\Delta f\}$ is carried out by

$$\{\Delta f\}=[k_t]\{\Delta\bar{u}_n\} \tag{40}$$

with $\{\Delta\bar{u}_n\}=\langle 0,0,\Delta\alpha_1,\Delta\bar{\delta},0,\Delta\alpha_2\rangle^T$ being the incremental natural deformations of the member, which can be expressed in terms of the incremental nodal displacements as follows (Yang and Kuo 1994):

$$\Delta\bar{\delta}\equiv L_2-L_1=\frac{1}{L_1+L_2}[2L_1(\Delta u_2-\Delta u_1)+(\Delta u_2-\Delta u_1)^2+(\Delta v_2-\Delta v_1)^2] \tag{41}$$

$$\Delta\alpha_1=\Delta\theta_1-\tan^{-1}\frac{\Delta v_2-\Delta v_1}{(L_1+\Delta u_2-\Delta u_1)} \tag{42}$$

$$\Delta\alpha_2=\Delta\theta_2-\tan^{-1}\frac{\Delta v_2-\Delta v_1}{(L_1+\Delta u_2-\Delta u_1)} \tag{43}$$

In Eqs. (41)-(43), L_2 and L_1 (=L) represent, respectively, the lengths of the member at the current and last obtained configurations. It is worth noting that the member end forces $\{f_1\}$ and $\{f_2\}$ in Eq. (39) are referred to their own member axes.

5. Examples

The accuracy of the proposed method has been verified in Tsou (1997) through many examples although only three of them are reported here. For all the presented examples, a column is discretized into four elements and a beam one element, and all external loads are applied proportionally. The reason why one column is modeled using four elements is that the frames analyzed are all sidesway allowed and the geometric nonlinearity effect of columns is important for this type of frame. The conventional geometric stiffness matrix, which is derived on the basis of cubic shape functions, cannot capture such nonlinearity very accurately if only one element per column is used. In this case our numerical experience indicates that the ultimate strength may be overestimated by up to five percent. Also, unless otherwise stated, members are W8×31 sections with the residual stress pattern as depicted in Fig. 2, where $\sigma_{rc}=0.3\sigma_y$.

5.1 Kanchanalai portal frame

Consider the Kanchanalai portal frame of Fig. 10 (Kanchanalai 1977). Strength interaction diagrams for bending about the major and minor axes obtained using the proposed method are plotted and compared with Kanchanalai's plastic-zone results in Figs. 11(a) and (b). From these figures excellent agreement between both results can be observed for both major- and minor-axis bending.

5.2 Kanchanalai leaned frame

Consider the Kanchanalai leaned frame of Fig. 12 (Kanchanalai 1977, Attalla *et al.* 1994). Comparisons of interaction diagrams for bending about the major and minor axes are shown in Fig. 13. Clearly, the proposed method yields excellent results compared with Kanchanalai's plastic-zone results.

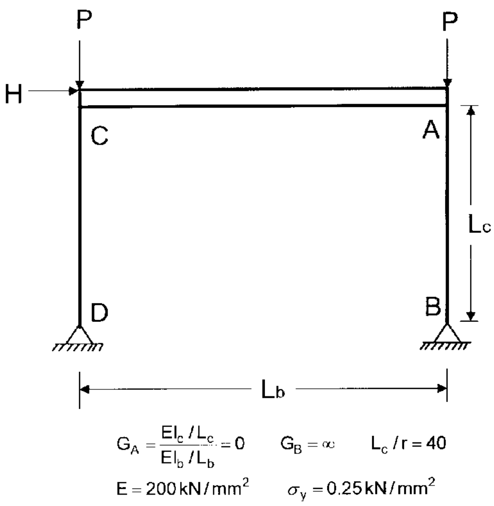

Fig. 10 Kanchanalai portal frame

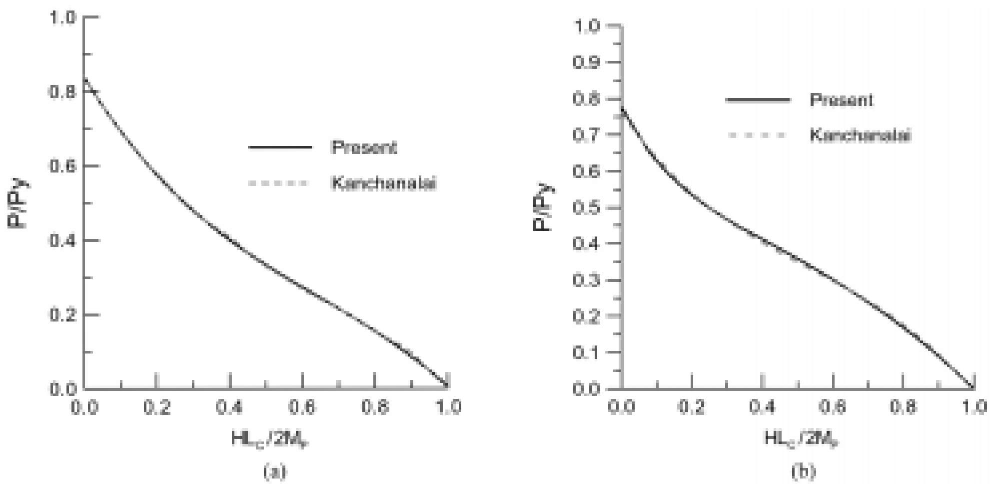

Fig. 11 (a) Strength interaction diagrams for Kanchanalai portal frame subjected to major-axis bending; (b) Strength interaction diagrams for Kanchanalai portal frame subjected to minor- axis bending

5.3 El-Zanaty portal frame

The portal frame depicted in Fig. 14 studied by El-Zanaty *et al*. (1980) has been shown to be sensitive to the spread of plasticity effect (King *et al.* 1992). Figs. 15(a) and (b) show the normalized load-deflection curves obtained by the proposed method and those obtained using the fiber element model and the conventional elastic-plastic hinge method (reproduced from Attalla *et al.* 1994). From these figures, the accuracy of the present method is verified again.

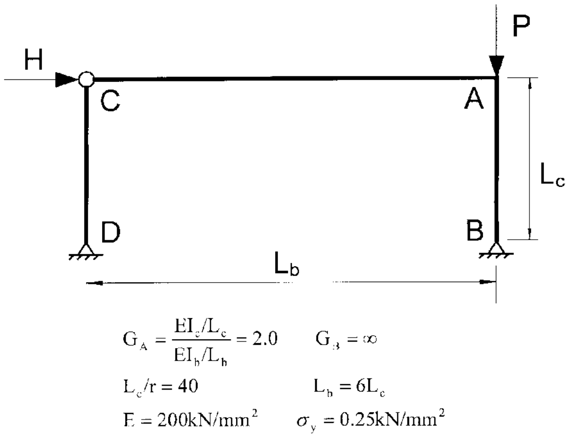

Fig. 12 Kanchanalai leaned frame

6. Discussions

6.1 Effect of coupling terms in elastic-plastic flexibility matrix

As mentioned in the introduction section, the elastic-plastic flexibility matrix derived by Attalla *et al.* (1994) is unsymmetrical. This is because both the reported normalized moment-curvature-axial force relationship $m(\phi, p)$ and the normalized centroidal axial strain-curvature-axial force relationship $\bar{\varepsilon}_0(\phi, p)$ are obtained by curve fitting the plastic zone results with respect to a W8×31 section; these two fitted relationships are inconsistent. The inconsistency means that for given values of ϕ

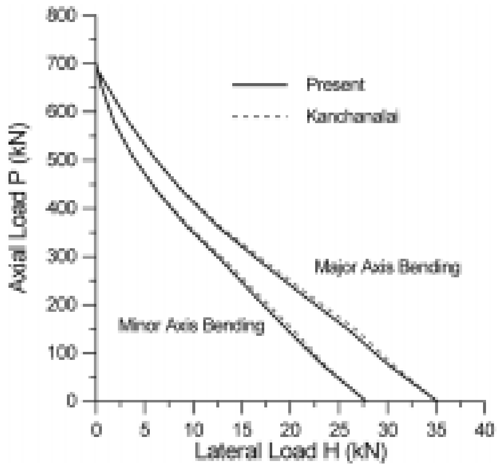

Fig. 13 Strength interaction diagrams for Kanchanalai leaned frame subjected to major- and minor-axis bending

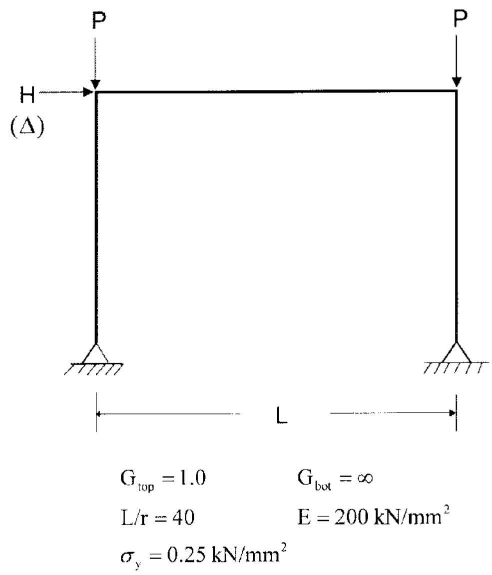

Fig. 14 El-Zanaty portal frame

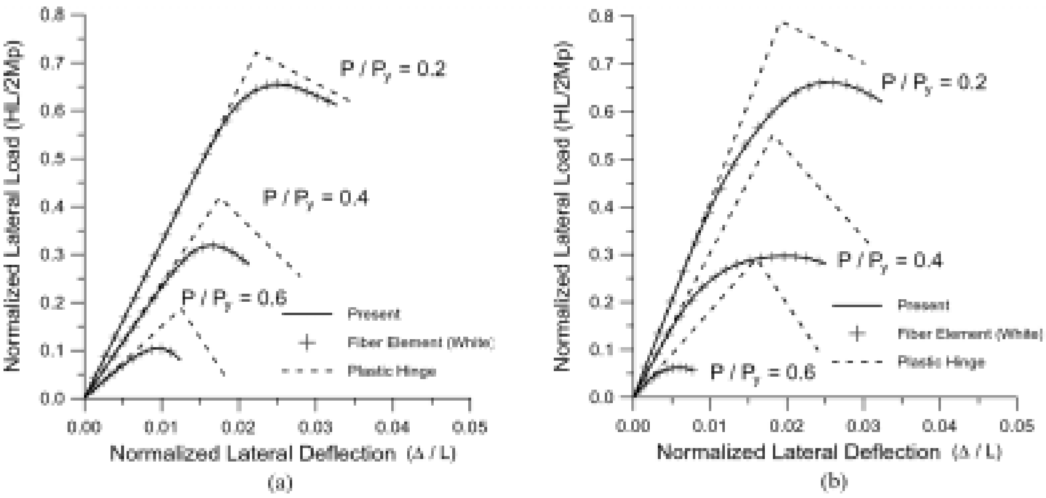

Fig. 15 (a) Comparison of normalized load-deflection curves for El-Zanaty portal frame subjected to major-axis bending, (b) Comparison of normalized load-deflection curves for El-Zanaty portal frame subjected to minor-axis bending

and p, the values of m and $\bar{\varepsilon}_0$ calculated according to $m(\phi, p)$ and $\bar{\varepsilon}_0(\phi, p)$ do not correspond to the same configuration (state). To fully appreciate this point, recall that the relationship $\bar{\varepsilon}_0(\phi, p)$ is a byproduct of the relationship $m(\phi, p)$ as discussed in Section 2.2. If these two relationships are approximate, the derived force-deformation relationships are also approximate, and this results in unsymmetrical elastic-plastic flexibility coefficients for the coupling terms, i.e., $d_{13} \neq d_{31}$ and $d_{12} \neq d_{21}$. Note that d_{32}=d_{23} even though the generalized stress-strain relationships are approximate. In the proposed method, it is found that the elastic-plastic flexibility matrix is always symmetric since the generalized stress-strain relationships are derived exactly and analytically.

To avoid the unsymmetry problem, Attalla *et al.* (1994) simply neglected the axial-flexural coupling terms by assuming d_{12}=d_{21}=d_{13}=d_{31}=0. However, it is unclear that whether the effect of these coupling terms is important. To investigate the effect, two versions of the proposed method are used, one with nonzero (exact) and the other with zero coupling terms. The analysis results, carried out with respect to the El-Zanaty frame bent about the minor axis with P=0.4P_y, are compared in Fig. 16. As shown in this figure, the ultimate strength is slightly overestimated if the axial-flexural coupling terms are assumed to be zero.

6.2 Effect of section sizes

Compared with the method proposed by Attalla *et al.* (1994), the proposed method is capable of considering the effect of section sizes explicitly in addition to having symmetric elastic-plastic flexibility matrix. This is because the generalized stress-strain relationships derived in this study are explicit functions of the section dimensions but these relationships in Attalla *et al.* (1994) are not although they are given in a nondimensional format.

To investigate the effect of section sizes, consider the El-Zanaty frame of Fig. 14 again with the following three sections: W8×31, W12×14, and W44×335, which represent typical medium, small, and large-size sections. The radii of gyration about the minor axis for these three sections are 2.02 in

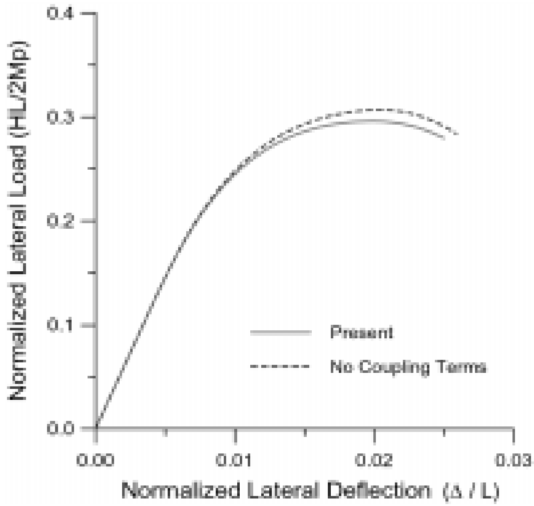

Fig. 16 Effect of coupling terms for El-Zanaty portal frame subjected to minor-axis bending with P=0.4P_y

(5.13 cm), 0.75 in (1.91 cm), and 3.49 in (8.86 cm), respectively. Note that for each case the slenderness ratio of the columns is still kept as 40. Figs. 17(a) and (b) show the normalized load-deflection curves with respect to the minor-axis bending for the column load P of 0.2P_y and 0.6P_y, respectively. It is seen clearly that the section sizes affect, to some extent, not only the ultimate strength but also the deformation associated with the ultimate strength especially when the column load is larger.

6.3 Simplification of elastic-plastic flexibility matrix

The elastic-plastic flexibility matrix given in Eq. (33) is based on the member force-deformation

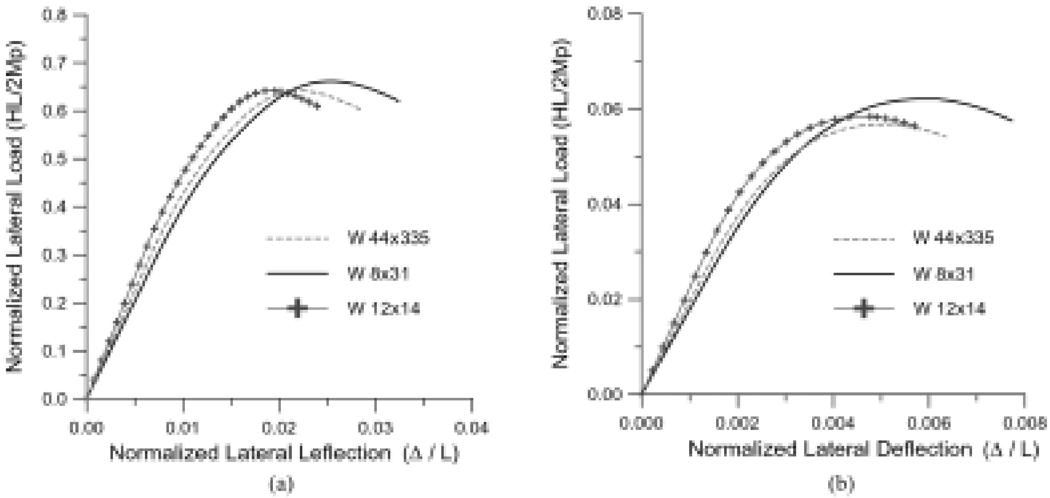

Fig. 17 (a) Effect of section sizes for El-Zanaty portal frame subjected to minor-axis bending with P=0.2P_y, (b) Effect of section sizes for El-Zanaty portal frame subjected to minor-axis bending with P=0.6P_y

relationships, which are in turn derived from the sectional moment-curvature-axial force and centroidal axial strain-curvature-axial force relationships. As the elastic-plastic flexibility matrix is symmetric and also the axial flexibility d_{11} is affected insignificantly by the effect of spread of plasticity, it is possible to obtain the elastic-plastic flexibility matrix without using the centroidal axial strain-curvature-axial force relationship as follows. First, simply let d_{12} equal d_{12} and let d_{13} equal d_{31}. Then, two methods are proposed for evaluating d_{11} approximately. Method one simply assumes that the axial flexibility does not change at all, i.e., $d_{11}=L/EA$. Method two calculates d_{11} according to the equation:

$$d_{11}=\frac{L}{EA}\frac{1}{2}\left(\frac{3EI}{L}d_{22}+\frac{3EI}{L}d_{33}\right) \tag{44}$$

Eq. (44) can be reasoned as follows. If the member is in the elastic state, its flexibility matrix will be of the form

$$[d]=\begin{bmatrix} \frac{L}{EA} & 0 & 0 \\ 0 & \frac{L}{3EI} & -\frac{L}{6EI} \\ 0 & -\frac{L}{6EI} & \frac{L}{3EI} \end{bmatrix} \tag{45}$$

After the member enters into the inelastic state, its flexibility will increase. Eq. (44) means that the inelastic axial flexibility is obtained from the multiplication of the elastic axial flexibility by an amplification factor which is taken to be the average of the amplification factors of the flexural flexibility coefficients d_{22} and d_{33}.

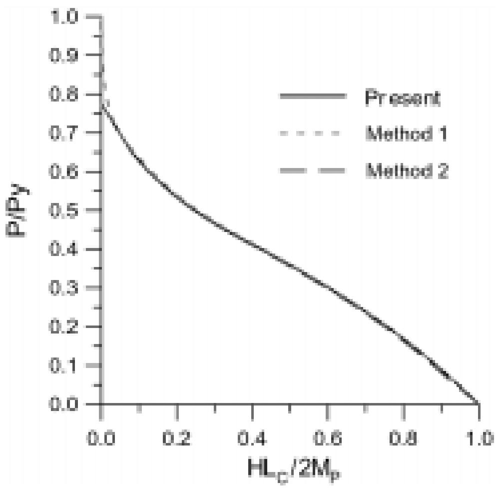

Fig. 18 Comparison of different methods for calculating axial flexibility considering Kanchanalai portal frame subjected to minor-axis bending

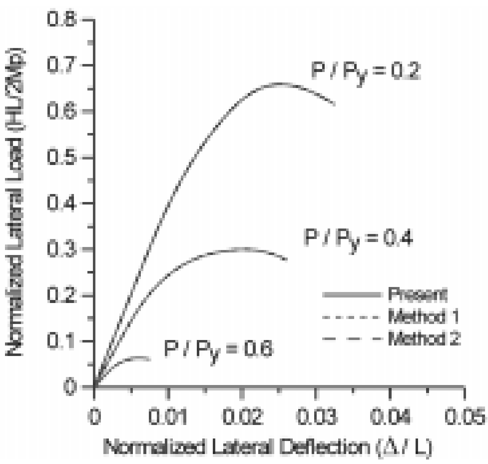

Fig. 19 Comparison of different methods for calculating axial flexibility considering El-Zanaty portal frame subjected to minor-axis bending

Comparisons of the accuracy of the two methods with that of the exact one (present) are given in Figs. 18 and 19, respectively, for the Kanchanalai portal frame and El-Zanaty frame, both bent about the minor axis. These figures show that method two is as accurate as the exact one and method one is also very accurate unless the axial force of columns is very large ($>0.75P_y$). Therefore, the strength of moment frames is not sensitive to how the axial flexibility is calculated and both proposed methods can be applied practically.

7. Conclusions

This paper has improved the quasi-plastic-hinge approach proposed by Attalla *et al.* (1994) in two aspects. First, it clearly shows that the unsymmetrical elastic-plastic flexibility matrix is due to the approximate generalized stress-strain relationships used in that paper. The proposed method employs exact generalized stress-strain relationships and therefore the derived elastic-plastic flexibility matrix is symmetric. Second, the proposed method is capable of considering the effect of section sizes explicitly and indeed such an effect may not be neglected as can be seen from the presented numerical example.

Moreover, two strategies are proposed in this paper to calculate the axial flexibility approximately so that the elastic-plastic flexibility matrix can be derived from only the moment-curvature-axial force relationship without needing the centroidal axial strain-curvature-axial force relationship. Numerical examples demonstrate that both strategies are very accurate. Finally, the proposed method is capable of modeling the effect of spread of plasticity very accurately and is also very efficient because only very few elements are needed to model a frame member.

Acknowledgment

This research was sponsored by the National Science Council of the Republic of China under Grant No. NSC 87-2211-E-002-032.

References

Attalla, M.R., Deierlein, G.G., and McGuire, W. (1994), “Spread of plasticity: Quasi-plastic-hinge approach”, *J. of Struct. Eng.*, ASCE, **120**(8), 2451-2473.

Attalla, M.R. (1995), “Inelastic torsional-flexural behavior and three-dimensional analysis of steel frames”, Ph.D. Dissertation, Cornell University, Ithaca, N.Y., USA.

Clarke, M.J., Bridge, R.Q., Hancock, G.J., and Trahair, N.S. (1992), “Advanced analysis of steel building frames”, *J. of Constr. Steel Res.*, **23**, 1-29.

El-Zanaty, M.H., Murray, D.W., and Bjorhovde, R. (1980), “Inelastic behavior of multistory steel frames”, Struct. Engrg. Rep. No. 83, Univ. of Alberta, Edmonton, Alberta, Canada.

Galambos, T.V., and Ketter, R.L. (1959), “Columns under combined bending and thrust”, *J. of the Eng. Mech. Div.*, ASCE, **85**(2), 1-30.

Kanchanalai, T. (1977), “The design and behavior of beam-columns in unbraced steel frames”, CESRL Report No. 77-2, Univ. of Texas, Austin, Texas.

King, W.S., White, D.W., and Chen, W.F. (1992), “Second-order inelastic analysis methods for steel-frame design”, *J. of Struct. Eng.*, ASCE, **118**(2), 408-428.

Liew, J.Y.R., White, D.W., and Chen, W.F. (1993a), "Second-order refined plastic-hinge analysis for frame design. Part I", *J. of Struct. Eng.*, ASCE, **119**(11), 3196-3216

Liew, J.Y.R., White, D.W., and Chen, W.F. (1993b), "Second-order refined plastic-hinge analysis for frame design. Part II", *J. of Struct. Eng.*, ASCE, **119**(11), 3217-3237.

Liew, J.Y.R., White, D.W., and Chen, W.F. (1994), "Notional-load plastic-hinge method for frame design", *J. of Struct. Eng.*, ASCE, **120**(5), 1434-1454.

McGuire, W., Gallagher, R.H., and Ziemian, R.D. (2000), *Matrix Structural Analysis*, John Wiley & Sons, New York.

Yang, Y.B., and Chiou, H.T. (1987), "Rigid body motion test for nonlinear analysis with beam elements", *J. of Eng. Mech.*, ASCE, **113**(9), 1404-1419.

Yang, Y.B., and Shieh, M.S. (1990), "Solution method for nonlinear problems with multiple critical points", *AIAA J.*, **28**(12), 2110-2116.

Yang, Y.B., and Kuo, S.R. (1994), *Theory and Analysis of Nonlinear Framed Structures*, Prentice-Hall, Singapore.

Teh, L.H., and Clarke, M.J. (1999), "Plastic-zone analysis of 3D steel frames using beam elements", *J. of Struct. Eng.*, ASCE, **125**(11), 1328-1337.

Tsou, C.H. (1997), "Second-order analysis of planar steel frames considering the effect of spread of plasticity", M.S. Thesis, Department of Civil Engineering, National Taiwan University, Taipei, Taiwan, ROC (in Chinese).

White, D.W. (1993), "Plastic hinge methods for advanced analysis of steel frames", *J. of Constr. Steel Res.*, **24**(2), 121-152.

White, D.W., Liew, J.Y.R., and Chen, W.F. (1993), "Toward advanced analysis in LRFD", *Plastic Hinge Based Methods for Advanced Analysis and Design of Steel Frames*, White, D.W. and Chen, W.F., eds., SSRC, Lehigh University, Bethlehem, PA.

Wolfram, S. *Mathematica: A System for Doing Mathematics by Computer*, 2nd ed., Addison-Wesley, Redwood City, CA.

Zhou, S.P., and Chen, W.F. (1994), "Plastic-zone analysis of beam-columns and portal frames", *Advanced Analysis of Steel Frames: Theory, Software, and Applications*, Chen, W.F. and Toma, S., eds., CRC press, Boca Raton, FL.